CGL Defect Chaos and Bursts in Hexagonal Rotating non-Boussinesq Convection

Santiago Madruga[+], Hermann Riecke[+], and Werner Pesch[*]
[+]*Engineering Science and Applied Mathematics, Northwestern University, Evanston, IL 60208, USA,* [*]*Physikalisches Institut, Universität Bayreuth, D-95440 Bayreuth, Germany*
(Dated: February 8, 2008)

We employ numerical computations of the full Navier-Stokes equations to investigate non-Boussinesq convection in a rotating system using water as a working fluid. We identify two regimes. For weak non-Boussinesq effects the Hopf bifurcation from steady to oscillating (whirling) hexagons is supercritical and typical states exhibit defect chaos that is systematically described by the cubic complex Ginzburg-Landau equation. For stronger non-Boussinesq effects the Hopf bifurcation becomes subcritical and the oscillations exhibit localized chaotic bursting, which can be modeled by a quintic complex Ginzburg-Landau equation.

PACS numbers: 47.52.+j,5.45.Jn,47.20.Lz,47.27.Te

The complex Ginzburg-Landau equation (CGL) as the universal description of weakly nonlinear oscillations has been studied theoretically in great detail. The classical, supercritical case, which involves only two independent parameters, looks deceptively simple. It exhibits, however, a vast variety of qualitatively different phenomena including different types of spatio-temporally chaos (e.g. [1, 2]). If the oscillations arise in a subcritical Hopf bifurcation the quintic CGL comes into play, which introduces further interesting states including, for instance, intermittent bursts in the oscillation amplitude.

In contrast to the extensive theoretical work on the CGL, direct experimental validation of its various regimes of complex behavior are rather scarce, in particular for the two-dimensional case [3]. In this paper we present detailed numerical computations for an experimentally realizable thermal convection experiment that exhibit defect chaos and bursts. We show that for the defect chaos the cubic CGL should provide a systematic description, while the bursts can be modeled with a quintic CGL.

Rayleigh-Bénard convection of a fluid layer heated from below in systems with large aspect ratio, in which the lateral dimension L of the layer is much larger than its thickness h, has proved to be a paradigmatic experimental system [4] for studies of complex patterns. Above a critical temperature difference ΔT_c across the layer, which corresponds to the critical value R_c of the dimensionless Rayleigh number R, one observes in the simplest case the familiar striped (roll) patterns with wavenumbers q close to the critical wavenumber q_c. However, in systems in which ΔT_c is large fluid properties like the thermal expansion coefficient or the viscosity vary significantly across the layer. Under these non-Boussinesq (NB) conditions the instability of the homogeneous state leads to hexagonal convection patterns [5].

If the chiral symmetry of the system is broken by rotating the layer about a vertical axis with frequency Ω, new interesting dynamics arise. For Ω above the Küppers-Lortz frequency Ω_{KL} one finds in the Boussinesq case immediately at onset R_c domain chaos in which rolls persistently switch orientation (cf. [4]). In contrast, in the NB case the hexagons are steady in this regime. However, weakly nonlinear theory predicts a secondary oscillatory instability at $\epsilon \equiv (R - R_c)/R_c = \epsilon_H$ that leads to 'whirling hexagons' in which the three hexagon amplitudes oscillate about their mean, with their phases shifted by $2\pi/3$ relative to each other [6, 7, 8, 9] (cf. Fig.1).

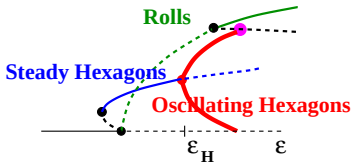

FIG. 1: Sketch of bifurcation diagram for rotating NB-convection. Solid (dashed) lines denote stable (unstable) branches. For the oscillating ('whirling') hexagons maxima and minima of the oscillations are indicated (thick solid lines).

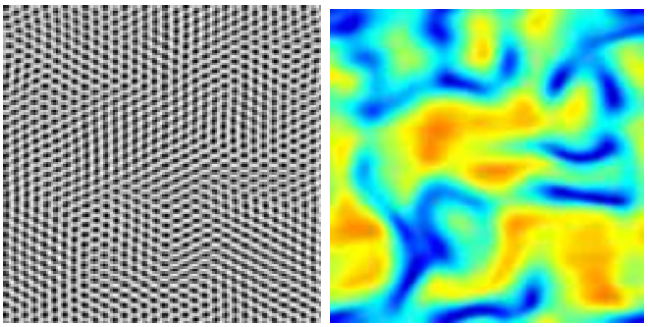

FIG. 2: Disordered state of whirling hexagons in case A for $\epsilon = 0.2$ ($R = 7396.6$), $L = 32 \cdot 2\pi/q_c = 38.3$. a) Snapshot of $\theta(\mathbf{r})$. b) Magnitude $|\mathcal{H}|$ of oscillation amplitude of snapshot shown in a). Red (blue) indicates large (small) values of $|\mathcal{H}|$.

Here we perform computer experiments on rotating non-Boussinesq convection with water as working fluid. The experimental realization of these simulations should pose no serious difficulty in presently available experimental setups. Focusing on the whirling hexagons, we

obtain different spatio-temporally disordered states, an example of which is shown in Fig.2a, and use the complex oscillation amplitude $\mathcal{H}$ (see (2) below) to interpret them in terms of suitable complex Ginzburg-Landau equations. The magnitude $|\mathcal{H}|$ is shown in Fig.2b.

Specifically, we consider two situations corresponding to weak and intermediate NB effects, respectively, and solve the full Navier-Stokes (NS) equations with leading-order NB effects included, as discussed previously [10, 11]. We obtain spatially periodic stationary hexagon patterns and test their stability using a standard Galerkin method. The temporal evolution of the states is then simulated with a pseudo-spectral code with periodic lateral boundary conditions [10, 11]. We consider two set-ups differing in the mean temperature T_0 of the fluid layer. In <u>case *A*</u> we choose $T_0 = 14°\mathrm{C}$ resulting in $\Delta T_c = 6.4°\mathrm{C}$ and a value of $Q = -2.2$ for Busse's NB parameter [5]; <u>case *B*</u> with $T_0 = 12°\mathrm{C}$ and $\Delta T_c = 8.3°\mathrm{C}$ is more non-Boussinesq and yields $Q = -3.62$ [22]. In both cases $h = 0.492\,\mathrm{cm}$ and $\Omega = 65\,\nu_0/h^2$ with ν_0 being the viscosity of the fluid in the mid-plane.

In <u>case *A*</u> we obtain above the Hopf bifurcation at ϵ_H states in which almost all convection cells are oscillating about a mean, but for general initial conditions the oscillations of different cells are out of phase with respect to each other. This is shown in Fig.2a where the solution is visualized by the deviation $\theta(\mathbf{r},t)$ of the temperature from the conduction profile in the mid-plane of the fluid layer. Here $\mathbf{r}$ denotes the horizontal coordinates. To extract the oscillations explicitly we make use of the fact that the underlying hexagon pattern itself is well ordered. We first demodulate each snapshot in space by writing

$$\theta(\mathbf{r},t) = \sum_{j=1}^{3} A_j(\mathbf{r},t)\, e^{iq_c\hat{\boldsymbol{n}}_j\cdot\mathbf{r}} + c.c. + h.o.t. \qquad (1)$$

Here the wavevectors $q_c\hat{\boldsymbol{n}}_j$ represent the three dominant wavevectors of the hexagons and *h.o.t.* denotes their harmonics. For strictly periodic stationary hexagon patterns the amplitudes A_j, $j = 1..3$, do not depend on $\mathbf{r}$ or t and have the same modulus A_{hex}. They can be chosen real and positive in our case (water). More generally, the amplitudes $A_j(\mathbf{r},t)$ depend slowly on space representing the contributions from the side-bands of the basic wavevectors $q_c\hat{\boldsymbol{n}}_j$.

Slightly above the Hopf bifurcation the amplitudes A_j vary in time. For patterns that are close to periodic in space they can be expressed as

$$A_j = \left(A_{hex} + \mu^{1/2}\left[e^{j\,2\pi i/3}\mathcal{H}\,e^{i\omega t} + c.c.\right] + \mathcal{O}(\mu)\right)\times \exp\left(i\Delta q\,\hat{\boldsymbol{n}}_j\cdot\mathbf{r} + i\mu^{1/2}\phi_j(\mathbf{r},t)\right), \qquad (2)$$

where $\mu = (R - R_H)/R_H$ and ω is the Hopf frequency. Here $\mathcal{H}$ denotes the complex oscillation amplitude, which we extract by standard demodulation of a series of snapshots like Fig.2a in space and time. The space dependence of the phases ϕ_j captures slight deformations of the underlying hexagon lattice.

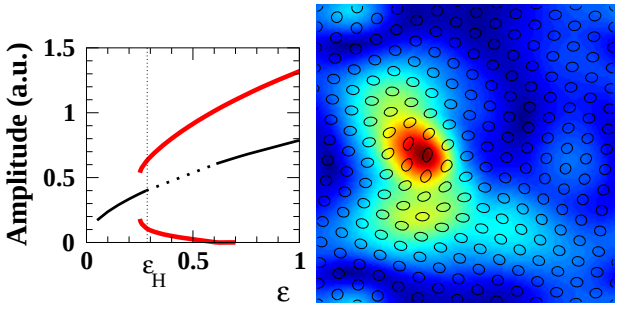

FIG. 3: a) Bifurcation diagram for the subcritical case *B* (cf. Fig.1 with the rolls omitted). b) Bursting state obtained with NS-simulation in case *B* for $\epsilon = 0.5$ ($R = 6121.9$) and $L = 16\cdot 2\pi/q_c = 19.1$. $|\mathcal{H}|$ color-coded as in Fig.2b, contour lines indicate hexagon pattern.

A representative snapshot of the magnitude of the oscillation amplitude is shown in Fig.2b. A more detailed analysis shows that the domains with low oscillation magnitude are due to spiral defects in the complex oscillation amplitude, i.e. $\mathcal{H} = 0$ at isolated points. During the evolution of the system these defects are persistently created and annihilated in pairs. In appearance, this state is thus quite similar to the defect chaos of the cubic CGL (see below).

When the NB effects are stronger (<u>case *B*</u>) the Hopf bifurcation is shifted to larger values of ϵ and, unexpectedly, becomes subcritical. The numerically determined bifurcation diagram showing the jump in the oscillation amplitude, the small hysteresis, and the restabilization (reentrance [11]) of the steady hexagons is presented in Fig.3a. As a consequence, the dynamical states obtained in this regime are very different, as shown in Fig.3b. The contour lines indicate the underlying hexagon pattern and, as in Fig.2b, the colors represent the oscillation magnitude. Strikingly, the oscillations are now localized into relatively small domains. Only within these domains the convection cells are elongated to footballs and are whirling. In most parts of the system the hexagons are relatively steady. The burst-like temporal evolution of the hexagon amplitudes is evident from Fig.4. It shows the normalized oscillation intensity in the bursts, which we define as $I(t) = N^{-1}\int_{|\mathcal{H}|>0.5|\mathcal{H}|_{max}} |\mathcal{H}|\,dxdy$ where N is the temporal mean of the integral. The intensity $I(t)$ exhibits substantial intermittency reflecting the growth and decay of bursts (thick solid line), while in case *A* (thin solid line) the intensity fluctuates relatively little.

To provide insight into the complex dynamics obtained in our numerical experiments we make use of the fact that the whirling hexagons arise from a Hopf bifurcation. It is therefore natural to expect that in the supercritical case the dynamics can be captured by the CGL for the oscillation amplitude,

$$\partial_T\mathcal{H} \;=\; \mu_2\mathcal{H} + d\nabla^2\mathcal{H} - c\mathcal{H}|\mathcal{H}|^2. \qquad (3)$$

We determine the linear coefficients μ_2 and $d \equiv d_r + id_i$ using the Galerkin stability computations and extract the

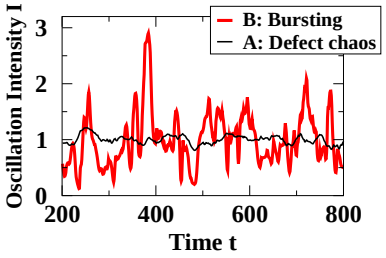

FIG. 4: Normalized oscillation intensity $I(t)$ (see text). Case A (thin black line) and case B (thick red line).

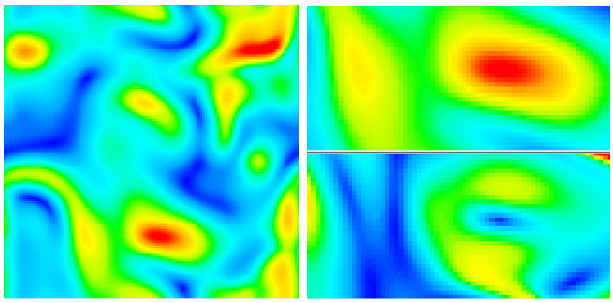

FIG. 5: Bursting state obtained with quintic CGL for parameters corresponding to Fig.3, $\mu_2 = 0.064$, $d = 1.90 + 0.033i$, $c = -1.10 + 7.19i$, $g = 3.61 + 1.46i$, except for the larger system size, $L = 100$. a) magnitude $|\mathcal{H}|$ of oscillation, b) enlarged portion from a): magnitude $|\mathcal{H}|$ (top) and associated wavenumber $|\mathbf{k}|$ of oscillation (bottom).

nonlinear coefficient $c \equiv c_r + ic_i$ from the dependence of the oscillation frequency on the oscillation amplitude. We find $d = 1.3 + 0.051i$ and $c = 0.95 + 9.16i$. Consistent with predictions based on a theory for small-amplitude hexagons [8, 9], these values position the system in the Benjamin-Feir-stable regime $(1 + d_i c_i / d_r c_r > 0)$ in which, however, defect chaos persists due to the wavenumber selection by the spiral defects [1, 2]. Indeed, we find in the NS-simulations that spatially homogeneous oscillations are stable. To reach the chaotic attractor shown in Fig.2 we employ initial conditions in which the oscillations are not synchronized across the system.

To capture the bursting dynamics found in the subcritical case B the CGL (3) has to be extended to include a quintic term, $-g|\mathcal{H}|^4\mathcal{H}$. Proceeding as in case A, we determine the coefficients of the resulting quintic CGL and simulate it in two dimensions. As shown in Fig.5a, which depicts a snapshot of the magnitude $|\mathcal{H}|$, we obtain quite similar bursts. Based on this qualitative agreement we use the CGL to gain further insight into the bursting found in the NS-simulations.

The burst mechanism can be elucidated by considering the local gradient of the phase of $\mathcal{H} \equiv \mathcal{R}e^{i\psi}$, i.e. the wavevector $\mathbf{k} \equiv \nabla\psi$ of the oscillations. Note that $\mathbf{k}$ is not related to the wavevectors making up the hexagon pattern. Gradients in $|\mathcal{H}|$ induce significant differential phase winding due to the strong amplitude dependence of the oscillation frequency ($|c_i/c_r| \gg 1$). This leads to a

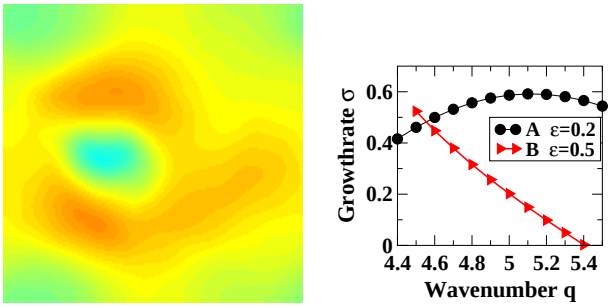

FIG. 6: a) $\nabla \cdot \vec{\phi}$ generated by burst shown in Fig.3b. b) Growth rate σ of the oscillatory mode as a function of the wavenumber $q = q_c + \Delta q$.

buildup of $|\mathbf{k}|$ at the perimeter of the bursts while $|\mathbf{k}|$ remains small at their cores, as illustrated in Fig.5b, which shows an enlargement of a burst (top) and the associated $|\mathbf{k}|$ (bottom). The increased wavenumber $\mathbf{k}$ enhances the dissipation via the diffusion term in (3) and eventually leads to a collapse of the oscillation amplitude. This mechanism has been studied previously in one dimension [12, 13, 14, 15, 16, 17]. It has been shown to underly the dispersive chaos observed in binary-mixture convection [13, 14] and, interestingly, can be strong enough to avoid blow-up even if there is no saturating nonlinear term at all ($c_r = g_r = 0$) [12, 15, 16]. The collapse can also be interpreted in terms of two colliding fronts that connect the steady base state with the nonlinear oscillatory state. Since these fronts select a non-vanishing wavenumber for the nonlinear state, the base state can invade the nonlinear state even above the Hopf bifurcation ('retracting fronts') [17]. Note that the collapse of the bursts described here is not due to a break-down of the underlying hexagonal structure [18, 19].

Assessing the validity of the CGL (3) and its quintic extension it is clear that for such a *secondary* Hopf bifurcation a systematic treatment must also include the coupling of the oscillation mode to slow, long-wave deformations of the hexagon lattice [23]. They are characterized by gradients in the phase vector $\vec{\phi} \equiv (\phi_1, (\phi_2 - \phi_3)/\sqrt{3})$ [8]. In particular, local deformations of the hexagon lattice enter (3) through an additional term $\sim \mathcal{H}\nabla\cdot\vec{\phi}$, which captures the dependence of the growth rate σ of the oscillations on local compressions of the lattice. Conversely, gradients in $\mathcal{H}$ drive $\vec{\phi}$ [8]. As a careful analysis of the NS-simulations shows, they lead to a decrease of $\nabla \cdot \vec{\phi}$ inside the burst, as shown in Fig.6a. This has the same effect on σ as a decrease in the wavenumber of the hexagons, $q_c \to q_c + \Delta q$ with $\Delta q = \nabla \cdot \vec{\phi}/2$, and therefore results in an increase in σ (see Fig.6b), providing a positive feedback that enhances the bursting activity compared to the quintic CGL.

Of course, the coupling of the oscillations to the underlying lattice exists also in the supercritical case shown in Fig.2. Consistent with the weakly nonlinear description of rotating hexagons [8, 9], we find, however, that in this

regime the growth rate σ depends only weakly on the local wavenumber of the hexagons (see Fig.6b) and varies by less than 10% across the system. We therefore suggest that the classic cubic CGL should describe whirling hexagons very well in the supercritical case A.

In conclusion, we have numerically investigated whirling hexagons that arise in rotating NB-convection and have identified two different regimes. In the weakly NB case the oscillations typically exhibit defect chaos and our analysis suggests that this state should be well described by the cubic CGL. Rotating NB-convection would then represent one of only a few experimentally realizable physical systems [3] in which at least one of the complex states of the two-dimensional CGL is accessible.

For stronger NB effects we found that the Hopf bifurcation becomes subcritical and typical states exhibit bursts. Such bursts and the related retracting fronts have been discussed in some detail previously in one dimension [12, 13, 14, 15, 16, 17]. The intermittent bursting behavior, however, has not been studied in detail yet. In two dimensions even less is known. For instance, the conditions for the persistence of bursting when stable steady and whirling hexagons compete remain to be understood. Preliminary simulations indicate that for $\epsilon = 0.7$ the bursting persists but not for $\epsilon = 0.9$ (cf. Fig.3a).

Since the oscillations arise in a secondary bifurcation the oscillatory mode is, in principle, coupled to the deformations of the hexagon lattice. While in the supercritical case our results indicate that this effect should be small, it is more significant in the subcritical case, where deformations of the lattice modify the growth rates of the oscillatory mode substantially (cf. Fig.6b). Compared to the bursting behavior of the quintic CGL alone, this leads to an enrichment of the scenario, which requires further investigations.

In our simulations we have taken great care to obtain defect-free hexagonal lattices. Since boundaries tend to introduce defects we have performed some runs in which circular ramps in the Rayleigh number mimic a circular container. By stabilizing the hexagon pattern near the boundary through an additional patterned volume heating we were able to recover the defect chaos and the bursting state. Conversely, it would be interesting to allow the underlying lattice to be disordered. In that case new phenomena may arise from the interaction of the penta-hepta defects with the whirling mode and significantly more complex states may be found (cf. [10]).

While our numerical experiments have been very productive in identifying and exploring various complex states in rotating NB-convection, current computational limitations do not allow us to use the NS-simulations to investigate in detail the statistical properties of these states. For instance, for the defect chaos we cannot address the possibility of deviations from the squared Poisson distribution for the defect statistics [20] or the expected transition to glassy states with exceedingly slow dynamics [21] as the wavenumber of the underlying hexagon pattern is changed [8]. Similarly, investigations of the ramifications of the hexagonal anisotropy due to the underlying lattice or of the broken chiral symmetry may require system sizes that are still beyond current computational capabilities. Questions like these can so far only be investigated in experiments.

Two of us (HR, WP) dedicate this paper to the memory of our good friend Lorenz Kramer.

We gratefully acknowledge support from the Department of Energy (DE-FG02-92ER14303).

[1] H. Chaté and P. Manneville, Physica A **224**, 348 (1996).
[2] I. S. Aranson and L. Kramer, Rev. Mod. Phys. **74**, 99 (2002).
[3] Q. Ouyang and J. M. Flesselles, Nature **379**, 143 (1996).
[4] E. Bodenschatz, W. Pesch, and G. Ahlers, Ann. Rev. Fluid Mech. **32**, 709 (2000).
[5] F. H. Busse, J. Fluid Mech. **30**, 625 (1967).
[6] J. W. Swift, in *Contemporary Mathematics Vol. 28* (AMS, Providence, 1984), p. 435.
[7] A. M. Soward, Physica D **14**, 227 (1985).
[8] B. Echebarria and H. Riecke, Phys. Rev. Lett. **84**, 4838 (2000).
[9] B. Echebarria and H. Riecke, Physica D **143**, 187 (2000).
[10] Y.-N. Young, H. Riecke, and W. Pesch, New J. Phys. **5**, 135 (2003).
[11] S. Madruga, H. Riecke, and W. Pesch, J. Fluid Mech. (to appear).
[12] L. M. Hocking and K. Stewartson, Proc. R. Soc. Lond. A **326**, 289 (1972).
[13] P. Kolodner, J. Glazier, and H. Williams, Phys. Rev. Lett. **65**, 1579 (1990).
[14] E. Kaplan, E. Kuznetsov, and V. Steinberg, Phys. Rev. E **50**, 3712 (1994).
[15] C. S. Bretherton and E. A. Spiegel, Phys. Lett. **96**, 152 (1983).
[16] W. Schöpf and L. Kramer, Phys. Rev. Lett. **66**, 2316 (1991).
[17] P. Coullet and L. Kramer, Chaos **14**, 244 (2004).
[18] M. Sano, H. Kokubo, B. Janiaud, and K. Sato, Progr. Theoret. Physics **90**, 1 (1993).
[19] K. E. Daniels, R. J. Wiener, and E. Bodenschatz, Phys. Rev. Lett. **91**, 114501 (2003).
[20] C. Huepe, H. Riecke, K. E. Daniels, and E. Bodenschatz, Chaos **14**, 864 (2004).
[21] C. Brito, I. S. Aranson, and H. Chaté, Phys. Rev. Lett. **90**, 068301 (2003).
[22] The NB coefficients (cf. [10, 11]) at threshold are given by $\gamma_0^{(c)} = 0.0009$, $\gamma_1^{(c)} = 0.2937$, $\gamma_2^{(c)} = -0.1681$, $\gamma_3^{(c)} = 0.0215$, $\gamma_4^{(c)} = -0.0022$ for case A and $\gamma_0^{(c)} = 0.0010$, $\gamma_1^{(c)} = 0.4885$, $\gamma_2^{(c)} = -0.2281$, $\gamma_3^{(c)} = 0.0287$, $\gamma_4^{(c)} = -0.0032$ for case B.
[23] It should be kept in mind that in contrast to the cubic CGL (3) the quintic equation can be derived rigorously from the underlying equations only if both c_r and c_i are

small. While this is generically not the case, it is useful to discuss the quintic CGL as a model equation.